A Microfluidic Chip with Integrated Colloidal Crystal for Online Optical Analysis

*Siew-Kit Hoi, Xiao Chen, Vanga Sudheer Kumar, Sureerat Homhuan, Chorng-Haur Sow, and Andrew A. Bettiol**

A microfluidic chip that incorporates colloidal crystals inside a microchannel system for on-chip integration of optical components is presented. It is demonstrated that the use of fluorescent spheres offers added advantages and functionality to the colloidal crystal array. Multifunctional optical components are demonstrated that are able to serve as a reference wavelength calibration line in measured reflectance spectra. Integrating colloidal crystals with varying filtering effects into a microfluidic chip enables selective transmission or blocking of a particular range of wavelengths locally. In addition, combinations of double-band colloidal crystal filters provide further tunability of the working wavelength for on-chip detection applications.

1. Introduction

There is an increasing trend towards adding functionality to lab-on-a-chip (LOC) devices through the integration of optics and optical components. This trend inevitably leads to the use of photonic and colloidal crystals because of their unique optical properties.[1–4] For example, recent work reported by Lee et al.[1] and Mandal et al.[2] has shown the potential of incorporating photonic crystals inside microfluidic channels for biochemical sensing and online photonic analysis. Lee et al. demonstrated a promising method for the incorporation of periodic photonic structures inside the microfluidic network using holographic lithography in combination with photolithography. The complexity and potential cost associated with using a top-down approach for incorporating 3D photonic crystals into a microfluidic channel can be overcome by utilizing the self assembly of colloidal crystals.

Over the last decade, colloidal photonic crystals prepared on different substrates have been used for a wide variety of applications. These include biological[5,6] and chemical sensors,[7–9] photonic paper,[10] optical switching,[11,12] reflective-type color displays[13,14] and colloidal crystal lasers.[15] In order to increase the functionality of colloidal crystals, fluorescent microspheres have been used as building blocks to form 3D-ordered films on glass substrates.[16,17] For these types of colloidal crystals, modified photoluminescence (PL) spectra were observed. However, to date, research into the integration of functionalized colloidal crystals with microfluidic LOC devices is still in its infancy.[3] Microfluidic channels with built-in colloidal crystals are an ideal platform that add functionality to LOC or micrototal analytical systems (μTAS) devices, enabling real-time analysis of ultrasmall amounts of biological and chemical samples. With improvements in microfabrication technologies, colloidal-crystal based microphotonic devices such as optical filters, lasers, and sensors that display specific optical properties can be realized. Integrating these features into a microfluidic chip will significantly improve the device performance in terms of reducing the processing time and size of the device, and also increasing the efficiency and sensitivity of the device.

Evaporation-induced self assembly of colloidal crystals inside a polydimethylsiloxane (PDMS) microchannel was first achieved by Kim et al.[18] Monodisperse microspheres were assembled into face-centered cubic (fcc) crystals within the rectangular microchannels. The self assembly of the microspheres was induced by the evaporation of water at the open ends of the microchannels.[19] More recently, Ozin et al. developed similar techniques with improved controllability and successfully assembled long-range ordering of opaline photonic crystals and its inverse opal structure with a very low concentration of intrinsic defects.[20–22] On the other hand, different methods have proven to be effective for preparing colloidal crystals inside a microchannel network. Moon et al. demonstrated colloidal crystallization in glass capillary tubes where colloidal silica microsphere suspensions were introduced by capillary action and crystallized by solvent evaporation from the other end.[23] Such colloidal crystals in capillary columns have been utilized by Kamp et al. to demonstrate the potential of colloidal crystals in combination with microfluidics for optical chromatography applications.[24] By infiltrating different alkanes with small refractive index variations into the colloidal crystals, a reflectance peak shift was detected. However, the drawback of using capillary tubes with an outer diameter of a few millimeters is that they cannot be easily integrated with other miniaturized devices because of their large size. In 2006, a fast, evaporation-free, colloidal self-assembly technique was introduced by

S.-K. Hoi, X. Chen, V. S. Kumar, S. Homhuan, Prof. C.-H. Sow
Prof. A. A. Bettiol
Department of Physics
National University of Singapore
117542, Singapore
E-mail: phybaa@nus.edu.sg

DOI: 10.1002/adfm.201002632

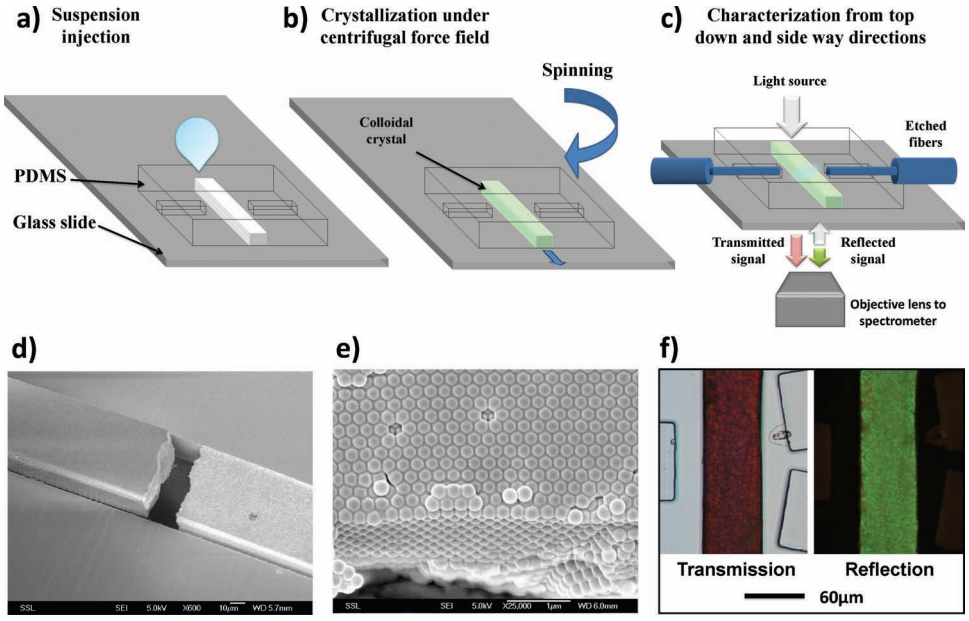

Figure 1. a–c) Schematics of the fabrication and characterization of colloidal crystal microfluidic chips. d–f) SEM and optical images of colloidal crystals confined in a microchannel, self-assembled from 220-nm PS microspheres. The cracking of the crystalline structure in (d) appeared when the sample was peeled off from the glass substrate. Trenches were prepared for fiber insertion.

Lee et al. to prepare colloidal crystals in microfluidic chips under a centrifugal force field.[25] The processing time was significantly reduced whereas the lattice quality of the crystalline structure was preserved. The stop bands or the reflectance maxima of the colloidal crystal could be tuned by filling the microfluidic chip with solvent media of different refractive indices.

Here we present several microfluidic chip designs that combine colloidal crystal filters, microchannels for the flow of samples, and most notably optical fibers for introducing an excitation light source and a detection probe. In contrast to conventional top-down probing methods,[10,13,24,25] the optical properties of the colloidal crystalline structure were probed locally by using etched optical fibers that were positioned by structures patterned into the PDMS molds. This provides flexibility to our colloidal-crystal based filter that can readily be combined with other miniaturized microfluidic components, rendering improved potential in lab-on-a-chip devices or micrototal analytical systems. Integrating colloidal crystals with different filtering effects into the microfluidic chip enables the selective transmission or blocking of a particular range of wavelength locally. In addition, using different combinations of double-band colloidal-crystal filters provides further tunability of the working wavelength for on-chip detection applications.

2. Results and Discussion

Figure 1a–c shows a diagram of the procedure employed to prepare the colloidal crystal in the microfluidic chip along with the integrated optical fiber. The chip was fabricated in polydimethylsiloxane (PDMS) using soft lithography from a master mold that was fabricated in SU-8 using the proton-beam writing technique.[26] Proton-beam writing is a powerful lithography technique that is particularly well suited to fabricating a master mold with high aspect ratio and smooth side walls. A drop (20 μL) of polystyrene (PS) microspheres suspension was injected into the reservoir that was connected to a microchannel. Afterwards, the inlets were sealed up with polyimide tape (Capton film, 3M) to ensure that the suspension flows through the microchannel during the spinning process.

Before the spinning of the device, the microfluidic chip was placed in ambient air for 5 minutes so that the colloidal particles began to crystallize near the open ends of the channel through the evaporation of water in the suspension. Afterwards, the microfluidic chip was spun with a rotation speed of 2000 revolutions per minute (rpm). The colloidal spheres were driven continuously by the centrifugal force to the end of the channel and ordered into the lattice of the growing crystal. Typically a crystal length of 1 cm could be formed in a 40-μm high and 60-μm wide channel after 30–60 minutes.

Scanning electron microscopy (SEM, JEOL JSM-6400F) performed on both the surface and the cross section of the crystalline structure revealed that the colloidal crystal formed inside the microchannel assembled into a face-centered cubic (fcc) structure. Representative SEM images of the hexagonal packing are shown in Figure 1d,e. Figure 1d shows a low-magnification image of the colloidal crystal confined to the rectangular microchannel. The cracking of the crystalline structure occurred when the sample was peeled off from the glass substrate. The crystalline structures were oriented with their [111] direction perpendicular to the glass substrate. Structural characterization studies performed by SEM (Figure 1e) confirm that the ordering extends over all three dimensions and the quality of the lattice is preserved even if the thickness of the crystal was increased to 40 μm. Shown in Figure 1f are optical images of the colloidal crystals taken in both transmission and reflection

when the incidence of the white light was normal with respect to the [111] planes of the confined crystal. Along the [111] direction, the periodic change of the dielectric constant results in a pseudo gap that can partially suppress the density of states for a certain band of frequencies. As a result, a different structural color is displayed by the crystalline colloidal array if an appropriate sphere size is used (200–300 nm). According to the Bragg equation,[27] the refractive index n, the spheres' diameter D, and wavelength of the reflected color λ are represented by:

$$\lambda = 2n_{\text{eff}}\ d_{111}\ \sin\theta \tag{1}$$

where, λ is the wavelength of the reflected light, n_{eff} is the effective refractive index, d_{111} is the structural period in the [111] direction, and θ is the incident angle to the [111] plane. The relationship between the diameter of the spheres D and the interplanar distance in the [111] direction d_{111} is given by:

$$d_{111} = \sqrt{\frac{2}{3}}D \tag{2}$$

and the effective refractive index is:

$$n_{\text{eff}} = \sqrt{f_{\text{m}}n_{\text{m}}^2 + (1 - f_{\text{m}}) \cdot n_{\text{p}}^2} \tag{3}$$

Here, n_{m} and n_{p} represent the refractive indices of the medium and the particle, respectively, and f_{m} denotes the void fraction (0.26 for fcc crystals). Hence, for PS spheres ($n_{\text{p}} = 1.59$) with a diameter of 220 nm in the dry form, $n_{\text{eff}} = 1.46$, and the wavelength of the reflected color can be deduced to be 524 nm. The colloidal crystalline array appears to be dark red and green in the transmission and reflection modes, respectively, which in good agreement with the Bragg equation (refer to Figure 1f).

The photonic band structure of a colloidal crystal can be probed experimentally by measuring its reflectance and transmittance spectra. By changing the refractive index of the medium that fills the voids of the crystalline structure, one can tune the photonic bandgap as the effective refractive index n_{eff} is modulated according to Equation 3. As depicted in **Figure 2**a, peaks in the reflectance spectrum shift to a longer wavelength position when a solvent of different refractive index was infiltrated into the microfluidic channel with a colloidal crystal. The reflectance spectrum in the dry form was broad and peaked at 520 nm. When water was filled into the microchannel, the spectrum narrowed and the peak shifted to 545 nm. A sharp spectrum with a peak at 550 nm was obtained when hexadecane ($n_{\text{m}} = 1.43$) was infiltrated into the colloidal crystal. The inset of Figure 2a shows the optical image of the reflected color for a 220-nm PS colloidal crystal infiltrated with hexadecane. Microscope immersion oil ($n_{\text{m}} = 1.52$) shifted the peak to 560 nm. It should be mentioned that as the refractive index contrast is smaller, the peak width will decrease.[5,28] Hence, here we observe a narrowing of the peak width which is related to the increase in the refractive index of the medium. The modulation of the stop-band maxima by the refractive index of the liquid may find applications in chemical or biosensing, such as on-chip detection of biomolecules that change the refractive index of a solution. The built-in colloidal crystal in the microfluidic network can be an indicator for the change in refractive index or buffer concentration. Micrototal analytical systems (μTAS) with on-chip cell culturing may benefit from such an integrated indicator which would offer online monitoring of the culturing environment.

Comparison of the spectra also reveals that introduction of the solvent inside the channel not only narrows the reflectance spectra, but also enhances the transmission signal. Figure 2b shows the transmittance spectra and optical images before and after infiltrating the interstices with hexadecane (refractive index 1.43). Using the same intensity of incident light, the transmittance spectra after introducing hexadecane display a red shift in the sharp dip and a higher intensity for the transmitted light is observed. This arises from the fact that the presence of hexadecane in the interstices of the colloidal crystalline array reduces the refractive index contrast and, hence, reduces the scattering loss caused by the interface between colloids, side wall, and medium.[28] The enhanced signals improve the performance of the microdevices. One added advantage of using a microfluidic channel is that hexadecane will remain in the confined channel for months even without any sealing of the channel.

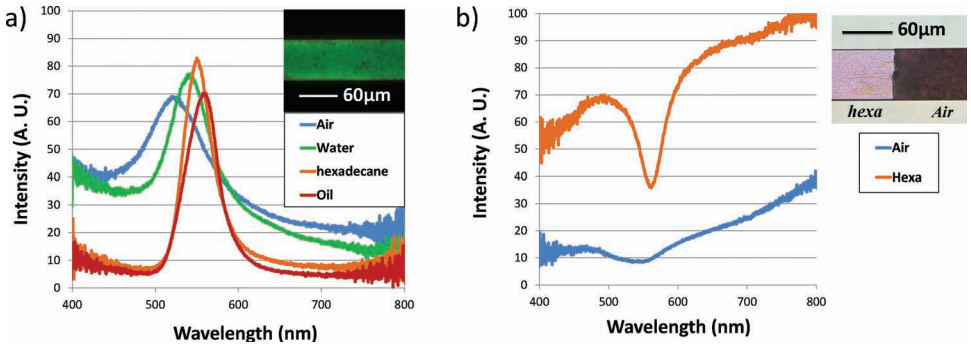

Figure 2. a) Modulations of optical reflectance spectra of the colloidal crystal in response to changing the solvent media (with different refractive indices). The spectra are narrower and red-shifted when liquid is infiltrated into the interstices of the crystal. All measurements were made at normal incidence to the colloidal crystal. The inset shows the optical microscopy image when hexadecane is infiltrated. b) Filling hexadecane into the microchannel enhanced the transmission signals. The inset shows the optical image of the colloidal crystal before and after infiltrating hexadecane into the crystalline structure.

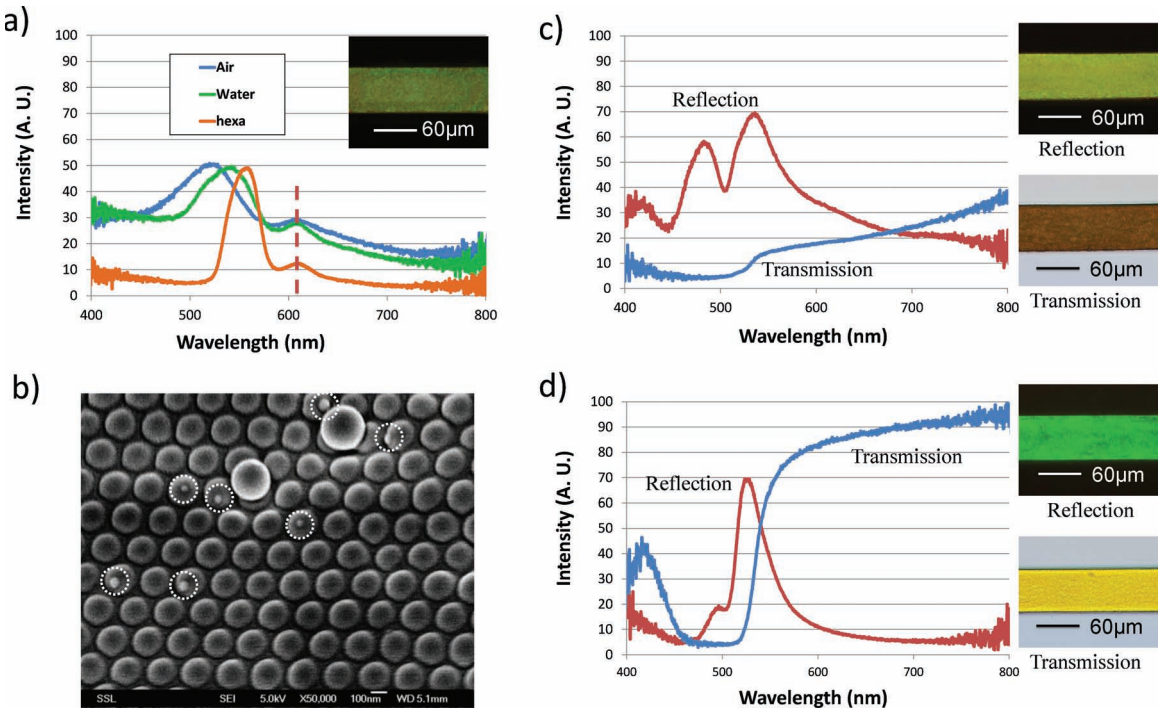

Figure 3. a) By filling the microchannel with different solvent media, the main peaks of the multifunctional optical components are shifted, whereas the small peaks remain at the same spectral position. The inset shows the optical image in dry form when 20-nm red fluorescent spheres (580/605) were added. b) SEM images of the colloidal crystalline structure of 220-nm PS spheres in the presence of 20-nm red fluorescent spheres (580/605) as indicated by the dotted circles. c,d) Reflectance and transmittance spectra and optical images of colloidal crystal formed by yellow green (YG) fluorescence-coated spheres (210 nm diameter, 505/515) before and after hexadecane was infiltrated, respectively. Fluorescent spheres with an absorption peak at 505 nm were chosen so that there was an overlap with the stop band of the crystalline array. As a result, the broad peak splits into two smaller peaks.

Using polystyrene spheres with a fluorescence coating can introduce additional optical components to the ordinary spectra. **Figure 3**a shows the reflectance spectra of a colloidal crystal formed from a mixture of ordinary polystyrene spheres with a diameter of 220 nm (concentratrion 2.36% solids in mixture) and red fluorescent nanospheres (580/605 – excitation at 580 nm; emission at 605 nm) with a diameter of 20 nm (concentratrion 0.2% solid in mixture). The inset in Figure 3a shows the optical microscopy image of the colloidal crystal formed from the mixture. The presence of the fluorescent nanospheres gave rise to an additional small optical peak at 605 nm in the reflectance spectra. The small peak at 605 nm came from the intrinsic optical property of the red fluorescent spheres with a diameter of 20 nm. The main peak was the result of the crystalline colloidal array of spheres with a diameter of 220 nm, which is consistent with the reflectance peak (blue) shown in Figure 2a. The SEM image shown in Figure 3b illustrates that the low-concentration 20-nm spheres did not affect the hexagonal closed packing of the crystalline structure. The nanospheres (circled) are scattered randomly in the sample. From our experiments, 0.2% of fluorescent nanospheres in the mixture was found to be optimal for reproducing the crystalline structure of the multifunctional components. If the concentration of the nanospheres in the mixture was too high (>0.2%), we observed that excessive nanospheres would be driven by the centrifugal force to the open end of the channel, forming a small segment with fluorescent particles. A lower concentration (<<0.2%) gave rise to a reduction in the peak height of the fluorescence signal. By filling the microchannel with different solvent media, the main peaks of the multifunctional optical components were shifted, whereas the small peak remained at the same position. As depicted in Figure 3a, the vertical dotted line marks the wavelength position of the unshifted peaks in the reflectance spectra.

The second example is the use of fluorescent spheres (210 nm diameter, 505/515) to form the colloidal crystal. Figure 3c and insets show the optical spectra and microscopy images in both the reflection and transmission mode. Fluorescent spheres with an absorption band peaking at 505 nm were chosen so that the peak overlapped with the stop band of the crystalline array. The broad peak that originated from the photonic bandgap splits into two because of the absorption at 505 nm by the fluorescence material. Consequently a sharp dip in the reflectance spectrum was observed. When the colloidal crystal was infiltrated with hexadecane, as shown in Figure 3d, the reflectance spectrum narrowed and shifted to a longer wavelength but the absorption at 505 nm remained unchanged as it is an intrinsic property of the fluorescent spheres. The absorption spectrum is thus a result from the colloidal crystal stop band that is split by the absorption from the fluorescent spheres. Only the stop band is affected by the change in the dielectric environment that occurs during infiltration with a solvent, and, hence, the position of the reflectance dip at 505 nm remains the same.

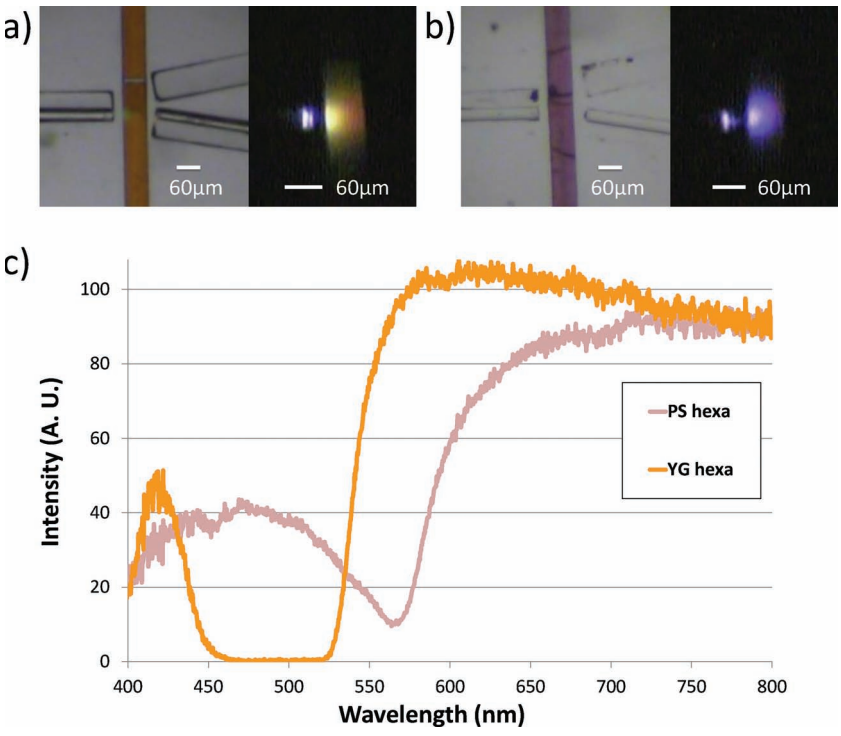

Figure 4. a) Top view of the colloidal-crystal based filter made from YG fluorescent spheres. White light guided by the fiber on the left hand side turns into red after passing through the 60-µm wide crystalline structure. The width and height of the microchannel are 60 µm and 40 µm, respectively. b) Top view of the colloidal-crystal based filter made from PS spheres with a diameter of 220 nm. c) Transmittance spectra captured by embedded fibers. Colloidal crystal formed by yellow green (YG) fluorescent spheres (505/515) with a diameter of 210 nm showing a sharp slope, which has the potential to perform as a longpass filter. The spectrum in pink displays the transmittance of a colloidal crystal made from 220-nm PS spheres.

In transmission mode, the color of the crystalline structure changed from red to yellow as a result of the drastic increase in transmitted light in the yellow range. The enhanced transmittance and the corresponding sharp edge that were observed in the spectrum imply that such a colloidal crystal has great potential for filter applications.

In order to incorporate a colloidal crystal as built-in filter in a LOC device, an etched multimode fiber was utilized to guide a broadband light source, and a second fiber was used to collect the transmitted light. Optical fibers of 125 µm in diameter (jacket stripped) were etched to about 35 µm in diameter by hydrofluoric acid (HF) in 2–3 hours. The etched fibers were inserted into the trenches that were prepared for fiber insertion, as shown in the top view image in **Figure 4**a. All measurements were performed on the colloidal crystal that was infiltrated with hexadecane in order to obtain an enhanced signal. From Figure 4a, we can see that white light guided by the fiber on the left hand side turned red after passing through the 60-µm crystalline structure. Figure 4b illustrates the transmission of white light through a crystalline structure made from ordinary PS spheres (diameter: 220 nm). White light becomes blue and reddish after passing through the colloidal crystal. As depicted in Figure 4c, the transmittance spectrum of yellow green (YG, 505/515) fluorescent spheres (diameter: 210 nm) shows that such colloidal crystals are ideal candidates for built-in filters for µTAS devices, in particular for fluorescence detection. The filter is effective in blocking wavelengths in the range of 460–530 nm while allowing longer emitted wavelengths to pass through. As a comparison, the transmittance spectrum of ordinary PS spheres with a diameter of 220 nm is also shown in the same Figure and the effect of using fluorescent spheres is explicitly demonstrated. The measured transmittance spectrum for the colloidal crystal made from fluorescent spheres is the result of the combination of two different effects. The first is the stop band, which is related to the 3D periodic nature of the colloidal crystal, and the second is the absorption band, which occurs due to the fluorescent molecules in the spheres. The overlap of these two bands result in a sharper transmission edge at 530 nm and the improved ability to block wavelengths between 460–530 nm.

The YG (210 nm) colloidal crystal shown in Figure 4 was combined with a second microchannel and embedded fibers to form a microfluidic chip that can be used to perform on-chip filtering in a fluorescence detection experiment. As shown in **Figure 5**a,b a mixture of fluorescent beads (20 nm in size, emission peaks at 515 nm and 605 nm) was introduced into the microchannel on the left. The fiber on the left hand side guided the excitation laser of wavelength 473 nm to the channel in order to excite the fluorescent beads in the microchannel. As illustrated in Figure 5c, without the integrated filter (Figure 5a), a blue spectrum with relatively high peak at 515 nm and low peak at 605 nm was obtained. However, if the YG (210 nm) colloidal crystal was integrated into the channel (Figure 5b), the peak at 515 nm was significantly attenuated without loss of the 605 nm signal. Hence, by introducing such an integrated filter into a microfluidic device, the performance and applicability of LOC devices can be improved.

One can further modulate the transmitted signal from a broadband source by integrating two types of colloidal crystal with different bands. **Figure 6**a shows an example of a double-band colloidal crystal with both YG (210 nm) and PS (220 nm) colloidal crystals integrated into microchannels that were parallel to each other. This was achieved by filling the different types of spheres in separate reservoirs that were connected to the microchannels. Two etched multimode fibers were inserted, one served as a broadband incident light source and a second fiber served as a collector for the transmitted light. As shown in Figure 6b, incident white light passed through the double-band colloidal crystal with a certain range of wavelengths filtered. In Figure 6c, the transmittance spectra collected shows how the spectrum of a single-band YG colloidal crystal can be modulated with different combinations of double-band colloidal crystals. The original transmittance spectrum of the YG (210 nm) colloidal crystal displayed a small hump in the blue range (400–450 nm) and a sharp slope at around 530 nm (yellow spectrum

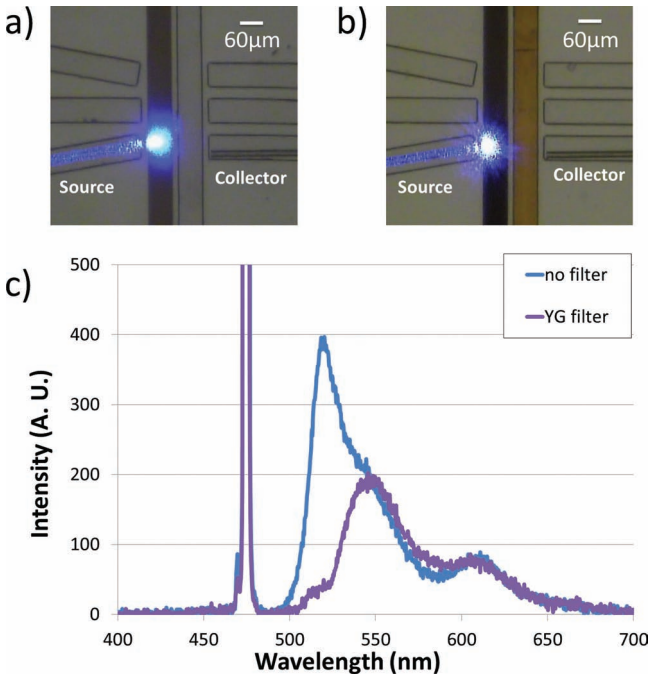

Figure 5. a,b) Top view of the microfluidic chip without and with integrated YG colloidal crystal filter, respectively. A blue laser (473 nm) was used to excite the mixture of fluorescent beads (20 nm, emission peaks at 515 nm and 605 nm) flowing in the channel on the left. c) Signal collected by the embedded fiber on the right hand side. As indicated by the purple spectrum, the integrated colloidal crystal filter has significantly attenuated the peak at 515 nm, while allowing signals of 605 nm to pass through.

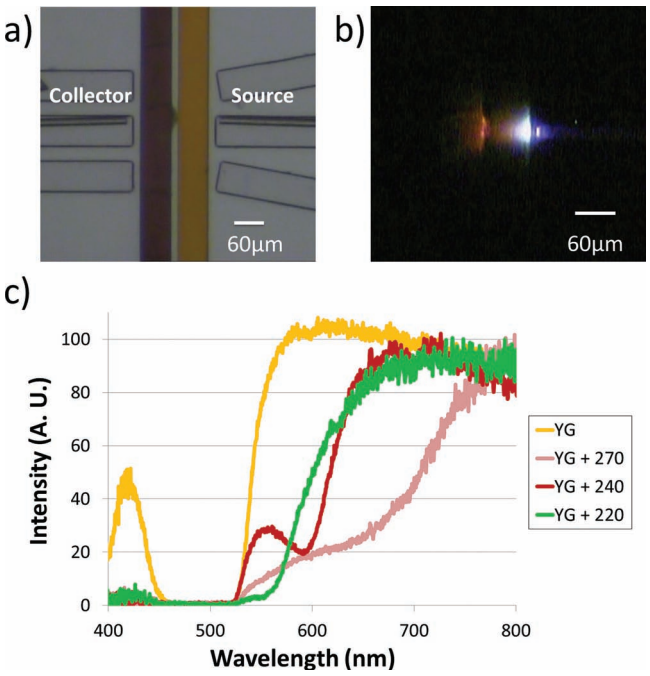

Figure 6. a) Top view of a double-band colloidal-crystal based filter. An etched multimode fiber was utilized to guide the broadband incident light source and a second fiber served as the collector of the transmitted light. b) Incident white light passed through the double-band colloidal crystal with a certain range of wavelengths filtered. c) The transmittance spectra collected show how the spectrum of a single-band YG colloidal crystal can be modulated using different combinations of double-band colloidal crystals.

in Figure 6c). The green spectrum was obtained when incident white light passed through a double-band colloidal crystal made from YG (210 nm) and PS (220 nm) spheres. We observed that in the new spectrum, the small hump in the blue range has been significantly attenuated and the slope has shifted from around 530 nm to around 560 nm. With reference to Figure 4c, we observed that the obtained spectrum is a result of the combined features from both spectra. The red spectrum was obtained when larger size colloids with a diameter of 240 nm were used in conjunction with the YG (210 nm) colloidal crystal. As shown, the additional stop band caused by the 240-nm colloidal crystal suppressed the transmittance at 600 nm and gave rise to a new spectrum. When a YG (210 nm) colloidal crystal was coupled with a colloidal crystal made from 270-nm spheres, the combined double-band crystal filtered most of the light in the visible range, only transmitting wavelengths in the near-infrared part of the spectrum. Further modulation of the transmittance can be achieved by using colloids of different sizes or by increasing the number of integrated bands of colloidal crystals.

3. Conclusion

The controlled preparation of colloidal crystals in a microfluidic system endows special optical and photonic functions to microfluidic devices. In this paper, we have successfully demonstrated a practical way of manufacturing photonic chips that integrate optical fibers, colloidal crystals, and microfluidic channels for LOC devices. Colloidal crystals made from yellow green (YG) fluorescent spheres (505/515) have been shown to have potential as built-in filters for μTAS. In addition, the combined double-band colloidal crystals also provide further tunability for filtering applications. Such integrated devices could be put into practice in actual LOC or μTAS devices.

4. Experimental Section

Fabrication of PDMS Microchannels: PDMS is a low-cost, silicon-based organic polymer that is routinely used in the fabrication of LOC devices by soft lithography.[29] First a master mold was fabricated in a layer of SU-8 photoresist that was spin coated onto a silicon wafer by using the proton-beam writing technique. After development of the SU-8 structure, a hard bake was performed to create a permanent, reusable master that could be used for soft lithography. PDMS molding was carried out in order to obtain the inverse structure of the master mold. The PDMS mold containing the microchannels was first cleaned using ethanol under sonication and then exposed to air plasma (Plasma Cleaner, Harrick Plasma) for 10 s in order to bond it to a glass slide.

Fabrication of Colloidal Crystal Chips: Commercial PS colloidal spheres (Polysciences, Inc) with an average diameter of 220 nm, 240 nm, and 270 nm (polydispersity of about 4%) were used. Red fluorescent spheres (580/605) with a diameter of 20 nm (Invitrogen, carboxylate modified, 2% solids) and yellow green fluorescent spheres (505/515) with a diameter of 210 nm (Invitrogen, carboxylate modified, 2% solids) were used to demonstrate multifunctional optical components. The mixture of PS

microspheres and fluorescence nanospheres used in the experiments for Figure 3a,b contained 0.2% of red fluorescent nanospheres and 2.36% of PS microspheres. The substrates employed were glass microscope slides (75 mm × 50 mm), which were subsequently cleaned with doubly distilled water, acetone, and isopropanol before being dried under a nitrogen gas flow. The PDMS microchannels were replicated with a soft-lithography technique and bonded to a glass slide after exposure to oxygen plasma. A spin coater (SPIN150-NPP) was used to spin the microfluidic chip at a rate of 2000 rpm for 30–60 minutes. The assembly of the colloidal crystal under centrifugal force was carried out at ambient temperature and atmosphere. The colloidal crystal formed inside the microchannel could be characterized immediately as the water solvent was removed under the strong centrifugal force. The infiltration of solvents into the packed channel was carried out using a vacuum desiccator. Before filling the solvent into the reservoir at the open end of the channel, the colloidal crystal chip was placed in a vacuum desiccator for 15 min. in order to remove the air inside the voids. This aided in expediting the solvent-infiltration process. The typical time for infiltration was 5–10 minutes if a vacuum desiccator was used.

Characterization: Optical images of colloidal crystal patterns were taken by a CCD camera (DS-RI1, Nikon) mounted on an inverted microscope (ECLIPSE T*i*, Nikon). Optical characterization was performed using an Ocean Optics USB2000 spectrometer attached to the eyepiece of the microscope, operating both in reflection and transmission mode. A halogen lamp was used as the light source. A 40x objective with a numerical aperture of 0.60 was used to illuminate the sample and collect the transmitted or reflected light at quasi-normal incidence with respect to the [111] planes of the colloidal lattice. A spatial filter was used to selectively detect light from a circular region with a diameter of about 30 μm. The optical reflectance spectra were observed from the bottom sides of the chips. We observed the modulation of the optical reflectance peaks by infiltrating the colloidal crystal confined inside the microchannels with various liquids. Hexadecane (98%, Sigma-Aldrich), immersion oil (Zeiss), and distilled water were used to give different refractive index mismatches relative to the colloidal particles.

Characterization from the edge was performed using etched multimode fibers (Thorlab, AFS50/125Y, Vis-IR) to guide a broadband incident light source (Mikropack DH-2000-BAL, UV–VIS–NIR) and to collect the transmitted light. The fiber insertion was carried out using a precision fiber optic positioning system (Newport, 561 ULTRAlign). Scanning electron microscope (SEM) images were taken by an SEM system (JEOL JSM-6400F). Before taking the SEM images, the PDMS channels were removed from the substrate and sputtered with a thin layer of platinum.

Acknowledgements

Funding support by the Singapore Ministry of Education (MOE) – Academic Research Fund (AcRF) Tier 2 Grant (R-144–000-258–112) is acknowledged.

Received: December 15, 2010
Revised: March 17, 2011
Published online: May 4, 2011

[1] S. K. Lee, S. G. Park, J. H. Moon, S. M. Yang, *Lab Chip* **2008**, *8*, 388.
[2] S. Mandal, J. M. Goddard, D. Erickson, *Lab Chip* **2009**, *9*, 2924.
[3] S. K. Lee, S. H. Kim, J. H. Kang, S. G. Park, W. J. Jung, G. R. Yi, S. M. Yang, *Microfluid. Nanofluid.* **2008**, *4*, 129.
[4] Y. J. Zhao, X. W. Zhao, Z. Z. Gu, *Adv. Funct. Mater.* **2010**, *20*, 2970.
[5] Y. J. Zhao, X. W. Zhao, C. Sun, J. Li, R. Zhu, Z. Z. Gu, *Anal. Chem.* **2008**, *80*, 1598.
[6] Y. J. Zhao, X. W. Zhao, J. Hu, M. Xu, W. J. Zhao, L. G. Sun, C. Zhu, H. Xu, Z. Z. Gu, *Adv. Mater.* **2009**, *21*, 569.
[7] J. H. Holtz, S. A. Asher, *Nature* **1997**, *389*, 829.
[8] K. Lee, S. A. Asher, *J. Am. Chem. Soc.* **2000**, *122*, 9534.
[9] B. V. Lotsch, G. A. Ozin, *Adv. Mater.* **2008**, *20*, 4079.
[10] H. Fudouzi, Y. N. Xia, *Adv. Mater.* **2003**, *15*, 892.
[11] Z. Y. Xie, L. G. Sun, G. Z. Han, Z. Z. Gu, *Adv. Mater.* **2008**, *20*, 3601.
[12] C. E. Reese, A. V. Mikhonin, M. Kamenjicki, A. Tikhonov, S. A. Asher, *J. Am. Chem. Soc.* **2004**, *126*, 1493.
[13] A. C. Arsenault, D. P. Puzzo, I. Manners, G. A. Ozin, *Nat. Photonics* **2007**, *1*, 468.
[14] T. S. Shim, S. H. Kim, J. Y. Sim, J. M. Lim, S. M. Yang, *Adv. Mater.* **2010**, *22*, 4494.
[15] H. Yamada, T. Nakamura, Y. Yamada, K. Yano, *Adv. Mater.* **2009**, *21*, 4134.
[16] Y. Z. Li, T. Kunitake, S. Fujikawa, K. Ozasa, *Langmuir* **2007**, *23*, 9109.
[17] R. V. Nair, R. Vijaya, K. Kuroda, K. Sakoda, *J. Appl. Phys.* **2007**, *102*, 123106.
[18] E. Kim, Y. N. Xia, G. M. Whitesides, *Adv. Mater.* **1996**, *8*, 245.
[19] P. D. Yang, A. H. Rizvi, B. Messer, B. F. Chmelka, G. M. Whitesides, G. D. Stucky, *Adv. Mater.* **2001**, *13*, 427.
[20] G. A. Ozin, S. M. Yang, *Adv. Funct. Mater.* **2001**, *11*, 95.
[21] H. Miguez, S. M. Yang, G. A. Ozin, *Langmuir* **2003**, *19*, 3479.
[22] G. A. Ozin, K. Hou, B. V. Lotsch, L. Cademartiri, D. P. Puzzo, F. Scotognella, A. Ghadimi, J. Thomson, *Mater. Today* **2009**, *12*, 12.
[23] J. H. Moon, S. Kim, G. R. Yi, Y. H. Lee, S. M. Yang, *Langmuir* **2004**, *20*, 2033.
[24] U. Kamp, V. Kitaev, G. von Freymann, G. A. Ozin, S. A. Mabury, *Adv. Mater.* **2005**, *17*, 438.
[25] S. K. Lee, G. R. Yi, S. M. Yang, *Lab Chip* **2006**, *6*, 1171.
[26] J. A. van Kan, L. P. Wang, P. G. Shao, A. A. Bettiol, F. Watt, *Nucl. Instr. Meth. Phys. Res. B* **2007**, *260*, 353.
[27] D. M. Mittleman, J. F. Bertone, P. Jiang, K. S. Hwang, V. L. Colvin, *J. Chem. Phys.* **1999**, *111*, 345.
[28] S. H. Kim, S. Y. Lee, G. R. Yi, D. J. Pine, S. M. Yang, *J. Am. Chem. Soc.* **2006**, *128*, 10897.
[29] Y. N. Xia, G. M. Whitesides, *Angew. Chem. Int. Ed.* **1998**, *37*, 551.